IAC-11-C1.1.7

MISSION ANALYSIS OF ROBOTIC, LOW THRUST MISSIONS TO THE MARTIAN MOONS DEIMOS AND PHOBOS

Uwe Derz
EADS Astrium Space Transportation GmbH, Bremen, Germany
uwe.derz@astrium.eads.net

Andreas Ohndorf
German Aerospace Center (DLR), Wessling, Germany
andreas.ohndorf@dlr.de

Bernd Bischof
EADS Astrium Space Transportation GmbH, Bremen, Germany
bernd.bischof@astrium.eads.net

ABSTRACT

The Martian moons Deimos and Phobos are interesting targets for exploration missions, especially within the frame of a crewed Mars orbit mission. To minimize the risk to a crew and also to support EVA site selection, a robotic precursor mission should investigate both moons in advance. The focus of this study is on mission analysis of such a precursor mission that utilizes low-thrust propulsion, in particular Electric Propulsion, for the transfer to the Martian system.

We assumed a launch by a Soyuz Fregat in 2018 and a direct injection into an escape trajectory with a hyperbolic excess velocity $v_\infty = 0$ km/s. The spacecraft uses electric propulsion for the interplanetary transfer to Mars and also for spiraling down from an elliptic capture orbit to its destination. The mission analysis comprises dedicated missions to either Deimos or Phobos, and combined missions with Deimos as the primary target and, during a possible mission extension, Phobos as the secondary target.

We used two different electric engine types for this study, which represent a wide range of specific impulse I_{sp}. The employed thruster types were the Snecma PPS®1350-G with I_{sp} = 1,650 s and the Astrium RIT-22 in two configurations having I_{sp} = 3,704 s and I_{sp} = 4,763 s. Within the analysis, we varied the number of engines and the available electrical power, followed by a down selection of a system design.

In the second part of this study we investigated the implications of transfer time and thruster count on the mission itself caused by permanent degradation of the power and propulsion subsystems. Therefore we selected 15 state vectors of the nominal transfer trajectory and, starting from each of these 15 new initial states, optimized new minimum-duration transfers under the assumption of permanent engine failures or degraded solar cells.

INTRODUCTION

Within the frame of possible future space exploration activities beyond Low Earth Orbit (LEO), human spaceflight missions to Near Earth Asteroids (NEA) and later to the Martian moons are investigated by several space agencies. To prepare for such an endeavor and to lower mission risk, robotic missions should be sent prior to crewed missions to potential targets of interest. Such precursor missions could address scientific objectives, identify potential hazards to a crew, and also search for in situ resources. Astrium analyzed conceptual system designs at phase-0 level for such precursor missions with special emphasis on missions to the Martian moons Deimos and Phobos. A mission analysis was conducted to assess the potential benefit of Electric Propulsion (EP) for such missions.

MISSION OUTLINE

For the studied precursor mission we assumed a launch with a Soyuz Fregat launch vehicle in 2018. After a coast phase in LEO, the Fregat upper stage injects the spacecraft into a parabolic escape trajectory with $v_\infty = 0$ km/s. After successful check out, the spacecraft uses its electrical engines for the interplanetary transfer to Mars where it arrives with $v_{inf} = 100$ m/s. Then, it uses its monopropellant attitude control thrusters to insert into an equatorial, high-elliptical Mars orbit with an apoapsis of 100,000 km.
From this elliptical orbit the spacecraft uses its electrical engines to transfer to its destination. This study considered dedicated missions to Deimos or Phobos but also combined missions. In the latter case, Deimos is defined as the primary target, because it is the outer moon. The spacecraft first spirals from its Mars capture orbit down to Deimos. After investigating Deimos for about 120 days, it continues to spiral deeper into the Martian system towards Phobos. Also considering that the orbits of both moons are almost circular and have only small inclinations with respect to Martian equatorial plane, an intermediate stop at Deimos should be possible with only a small increase of the mission's ΔV. Tab. 1 gives an overview of the major characteristics of Deimos and Phobos. Especially, the dimensions of both moons, ranging within a few kilometers, are significantly lower than those of Lunar and are more comparable to large NEAs.

	Phobos	**Deimos**
Semimajor axis [km]	9,378	23,459
Sidereal orbit period [h]	7.685	30.288
Sidereal rot. period [h]	7.685	30.288
Inclination [deg]	1.08	1.79
Eccentricity [-]	0.0151	0.0005
Major axis radius [km]	13.4	7.5
Medium axis radius [km]	11.2	6.1
Minor axis radius [km]	9.2	5.2
Mass [10^{15} kg]	10.6	2.4
Escape velocity [m/s]	10.3-12.2	5.6-6.7

Tab. 1: Major physical characteristics of the Martian moons Phobos and Deimos and their respective orbits [1]

SPACECRAFT DESIGN

To estimate the available payload mass for the considered mission targets, a simplified spacecraft mass model, including the spacecraft avionics, power, thermal control, propulsion, and structure components, is sufficient.

Avionics

The spacecraft avionics consists of three parts:

- Guidance, navigation, and control (GNC) subsystem
- Communication subsystem

- Data handling subsystem

GNC includes the following components:

- 2 x Inertial measurement units (IMU)
- 2 x Star sensors
- 2 x Sun sensors
- 4 x Reaction wheels
- 1 x Range sensor
- 1 x Wide angle camera
- 1 x Navigation camera

Based on equipment data from [2][3][4], the GNC suite mass including margin is 59.3 kg.

The spacecraft uses an X-band link for nominal telecommand and monitoring as well as for science data downlink. Ka-band communication equipment is additionally foreseen for high-accuracy radio tracking experiments. The system includes:

- 1 x steerable high gain antenna with X-band and Ka-band frequency feed
- 2 x omnidirectional X-band low gain antennas
- 2 x X-/Ka-band transponder for tele-command, telemetry, two-way rainging, Doppler and Δ-Differential one-way range measurements
- 2 x X-band Traveling Wave Tube Amplifier (TWTA)
- 1 x Ka-band Solid Sate Power Amplifiers
- Radio Frequency Distribution Unit

According to [3], a communication subsystem mass of 41 kg is realistic. In addition, also the data handling subsystem described in [3] is assumed as baseline for this mission with a mass of max. 6 kg.

Power

The power subsystem has to provide sufficient power to all spacecraft subsystems during all mission phases. Thereby, the spacecraft subsystems can be divided into three groups:

- The spacecraft bus (the avionics in particular) has to operate during all mission phases. The ESA Concurrent Design Facility (CDF) team conducted a detailed power system analysis [3] for a NEO mission. Based on that, we assumed a continuous power consumption of the spacecraft bus of 550 We.
- The EP subsystems typically have power demands in the range of 3-19 kWe. Because we varied the number and type of employed electric engines, the propulsion system's power demand is different for each considered spacecraft configuration. In addition, we assumed operation of electric engines only in sunlight, which reduced the requirements on the spacecraft batteries significantly.
- The spacecraft's scientific payload consumes minimum electrical power during the transfer. For the operation at the target, we assumed a continuous power consumption of 50 W [5].

The electrical power source is a pair of steerable, triple-junction solar cell arrays with a conversion efficiency $\eta = 28$ %. Its power is:

$$P_R = W_R A \eta \qquad (1)$$

with:

P_R: Electrical power output at the solar distance R to the Sun

W_R: Area specific solar flux at R

A: Area of the solar array (always perpendicular to the incident sunlight)

η: Conversion efficiency

The conversion efficiency η depends on the solar cell temperature and thus on the solar flux. With increasing Sun distance, η increases due to the decreasing solar cell

temperatures caused by the reducing solar flux. To allow the determination of P_R, and assuming $\eta = \text{const.}$, we modeled the solar flux in equation (1) in dependence on the spacecraft's distance from the Sun R

$$W_R = W_E \times \left(\frac{R_E}{R} \right)^{1.8} \qquad (2)$$

with
R_E: Earth orbit radius
R: Spacecraft-Sun distance
W_E: Solar flux at 1 AU (1,370 W/m²)

The exponent in equation (2) of 1.8 is used as correction for the cell temperature (otherwise it would be physically 2).

Like for commercial communication satellites, our spacecraft's solar arrays consist of several solar panels. We varied the number of panels per wing between one and four and also used two different panel types to adapt the power system's output to the spacecraft's power needs. Tab. 2 gives an overview of the two solar panel types that we considered for this study. Their power outputs were estimated using equations (1) and (2), and we assumed areaspecific masses of 3.25 kg/m² (state of the art) and 2.6 kg/m² (near future). Those values derive from solar array data given in [4] and include the solar cells, the cover glass, and the carrying structure.

Solar Panel Type:	**Small**	**Large**
Length [m]	3.92	3.05
Width [m]	2.28	2.28
Power output @Earth [kWe]	2.66	3.42
Power output @Mars [kWe]	1.28	1.65
Mass [kg]	22.6	29.0

Tab. 2: Solar panel characteristic data

Generally, the power of the electric propulsion system is processed by the spacecraft bus power control unit and then by the EP power supply unit. To reduce occurring losses, our power subsystem architecture instead contains separate solar array segments of each solar wing (marked blue in Fig. 1) that connect directly to the EP power supply unit, preventing any second power processing. A second segment of the solar array (marked red) supplies the spacecraft bus. This segment has to provide the electrical power for the bus systems and for the payload. Considering their power requirements, the required solar array area of 3.4 m² was determined with equations (1) and (2) and 3.4 m² of each solar wing allocated for redundant spacecraft bus supply.

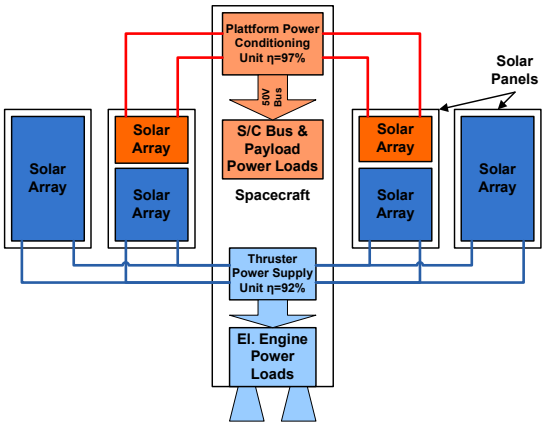

Fig. 1: Power subsystem architecture

Additionally, the power system contains the following elements

- Spacecraft bus power distribution and control unit (8 kg)
- Spacecraft bus battery (27 kg)
- Harness (30 kg)

Propulsion

We assumed a hybrid propulsion system, with EP for the interplanetary transfer and for

spiraling in the Martian Sphere of Influence (SOI); and chemical monopropellant propulsion for insertion into the high-elliptic Mars orbit, for injection into the orbits around the Martian moons, and for attitude control.

Two different types of electric engines have been considered as they represent a wide I_{sp}-range. The Snecma PPS®1350-G has a I_{sp} = 1,650 s and has been flight-proven in the ESA mission SMART 1. The second engine type, the Astrium RIT-22, is based on the flight proven RIT-10 (EURECA, ARTEMIS). Three designs of the RIT-22 with I_{sp} = 3,704 s, 4,763 s and 6,591 s are available. Using a RIT engine with I_{sp} = 6,591 s would require very large solar arrays, and the very high I_{sp} would only be beneficial for ΔVs higher than expected for Earth-Mars transfer. Hence, we considered only the PPS®1350-G and the RIT-22 with low and medium I_{sp} (RIT-22 LO, RIT-22 ME) for parametric investigations in this paper (Tab. 3). Please note, the relatively high minimal power consumption of the PPS®1350-G, which practically allows only limited throttling.

Engine	**PPS-1350**	**RIT22 LO**	**RIT22 ME**
Beam voltage [kV]	0.35	1.35	2.1
Specific impulse [s]	1650	3704	4763
Maximal power consumption [kWe]	1.5	4.02	6.2
Minimal power consumption [kWe]	1.2	2.6	4.03
Thrust [mN]	88	135.5	175
Thrust to power ratio [mN/kWe]	59.33	33.73	28.18
Mass incl. power processing [kg]	14.6	21.3	28.5

Tab. 3: Electric engine characteristics [2][6]

In addition to the thrusters, the EP system consists of the following components:

- Propellant tanks with two options
  - 96 l (Alenia), max. Xe-load 160 kg, dry mass 16 kg [7]
  - 133 l (PSI), used for the Bepi Colombo mission, max. Xe-load 212 kg, dry mass 20.6 kg [4]
- Propellant feeding system, 25 kg [3]

The chemical propulsion system consists of:

- 4 x 20 N hydrazine thrusters (I_{sp} = 224 s) for Mars orbit injection
- 8 x 1 N hydrazine thrusters (I_{sp} = 220 s) for attitude control
- 186 l hydrazine tank (PSI), 19.5 kg
- Propellant feeding system, 8 kg [3]

Thermal Control

The thermal control system must keep the interior of the spacecraft within a predefined temperature range. Therefore, it must radiate excess heat of the spacecraft's electrical equipment into space. Due to the high power needs of electric engines and the resulting waste heat, they have significant influence on the thermal control system design. A detailed thermal analysis of an EP-powered Mars mission gives [4]. This system can cope with a spacecraft power of 14.4 kWe, which is sufficient for most of the spacecraft configurations of this study. Because we conducted no detailed thermal analysis in this study, we used the thermal control system of [4] with a mass of 75 kg as reference.

Structure

Within this study, we did not carry out detailed structure analysis and therefore accounted the primary and secondary structure mass generally with 15% of the launch mass and added another 44 kg for mechanisms to the resulting 237 kg.

Launch

Our mission design foresees the Soyuz Fregat launch vehicle for the injection into a parabolic ($v_\infty = 0$ km/s), ecliptical escape trajectory. Because preliminary analysis showed a required launch declination of 30 deg, we chose a launch via an intermediate circular LEO, with the launch performance from [8] (Tab. 4). From a low-thrust mission analysis point of view, the higher spacecraft mass is regarded as worst case and baseline for the following trajectory calculations.

Launch site	**Baikonour**	**Kourou**
Launch performance [kg]	1850	1850
Performance margin [kg]	148	144
Launch vehicle adapter [kg]	120	120
Available spacecraft mass [kg]	1582	1536

Tab. 4: Launch vehicle performance and available spacecraft mass

MISSION ANALYSIS

We optimized all transfers of this paper with respect to minimum flight time, and we used the low-thrust optimizer InTrance (*In*telligent *Tra*jectory optimization using *n*euron*c*ontroller *e*volution) for this purpose [9]. This software combines Artificial Neural Networks (ANN) and Evolutionary Algorithms (EA) in a method named Evolutionary Neurocontrol (NC). The ANNs thereby steer a low-thrust spacecraft along its trajectory. The steering strategy is determined through the ANNs parameter set. A near-globally optimal solution is finally found after optimization of this parameter set by the EA. We used a Runge-Kutta-Fehlberg method (RKF54) for the integration of the Equations of Motion (EOM) and JPL's DE405 ephemerides for the state data of Earth and Mars. The nomenclature of our spacecraft configurations contains the 'number of engines', the 'engine type', and the 'EP power at 1 AU in kW', separated by a '-'.
For example, '2-RIT22ME-13.5' means two RIT-22 thrusters with $I_{sp} = 4{,}763$ s and 13.5 kWe electrical power available for propulsion at 1 AU Sun distance.

Interplanetary Transfer

We investigated low thrust interplanetary transfers with a launch date between 3rd September 2017 (58,000 MJD) and 30th June 2018 (58,300 MJD). To achieve a successful rendezvous with Mars, we required the spacecraft to reach the Martian SOI, which gives a maximum distance of approximately 580,000 km. This distance can in reality be reduced by executing comparably small midcourse correction maneuvers (MCM) far from Mars. We set the maximum allowed relative velocity at the SOI to 100 m/s.

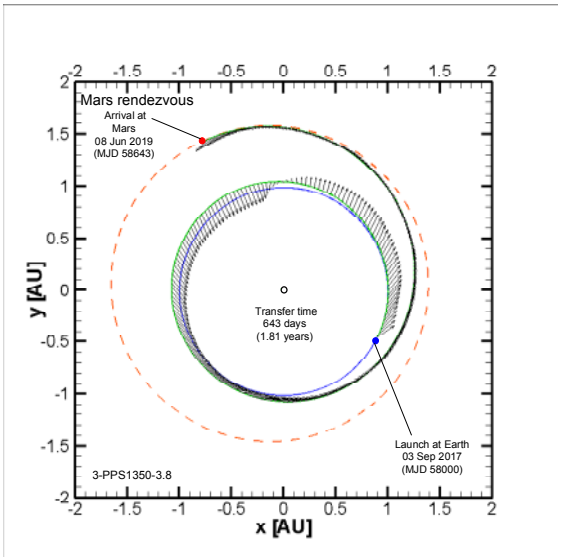

Fig. 2: Interplanetary transfer of the 3–PPS1350–3.8 spacecraft

Fig. 2 and Fig. 3 show two examples of low-thrust interplanetary transfers. The spacecraft configuration 3-PPS1350-3.8 can only provide an initial acceleration of 0.17 mm/s^2 at Earth. In addition, the small solar panels of this configuration lead to a significant thrust level reduction at larger Sun distances. Hence, the optimization leads to a 1.5-revolution transfer with a periapsis close to 1 AU where the solar array provides more power for the acceleration towards Mars. The same strategy is basically applied by the configurations 2-RIT22LO-8.7 and 2-RIT22ME-11.5.

In contrast, Fig. 3 shows how spacecraft configurations with larger solar arrays enabling 0.5-revolution transfers. Those transfers are desirable, because they have also a lower ΔV (Fig. 4). A further reduction in transfer time is possible with additional electric engines, larger solar arrays, or a combination of both. The effect is less pronounced (Fig. 5), though, and it has to be considered that a shorter transfer time usually goes along with an increased transfer ΔV.

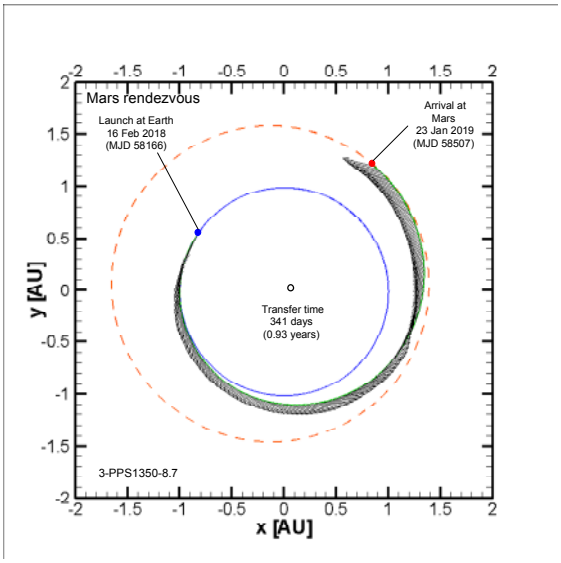

Fig. 3: Interplanetary transfer of the 3–PPS1350–8.7 spacecraft

An important aspect of the interplanetary transfer is the Sun distance at Mars arrival. All spacecraft configurations reach Mars between December 2018 and June 2019. Within this time window, Mars is still moving towards its aphelion on 26 August 2018. The power that is available for EP therefore still decreases during the following months when the spacecraft spirals within the Martian SOI.

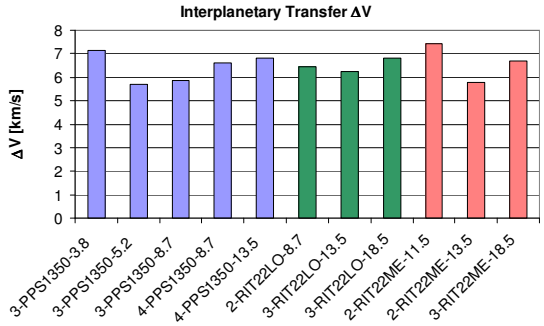

Fig. 4: Interplanetary Transfer ΔV (PPS1350 marked blue, RIT22LO: green, RIT22ME: red)

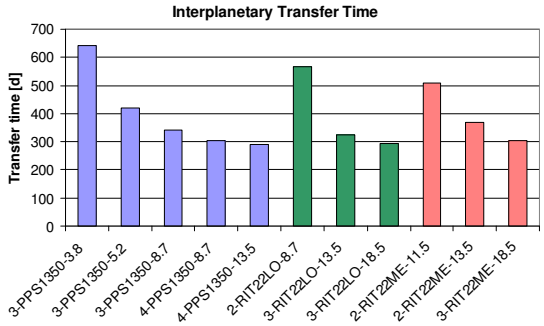

Fig. 5: Interplanetary transfer time

Mars Orbit Injection

To simplify the capture of the spacecraft, the electric engines switch off at the SOI's border, and a following, impulsive burn of the attitude control thrusters accomplishes the orbit injection. Compared to EP, the I_{sp} of those chemical monopropellant thrusters is low. To

keep the necessary ΔV for orbit injection as small as possible, the attitude control thrusters inject the spacecraft only into a high-elliptical Mars orbit with 100,000 km apocenter distance.

To determine the orbit injection ΔV, we conducted a two body orbit propagation of the inbound hyperbola and the first elliptical orbit in Matlab, using the ODE45 solver. A hyperbolic excess velocity of 100 m/s is the baseline for the nominal mission. However, equipment failures have been considered during later stage of this study. Engine cut offs or degradation of the solar panels, occurring during the interplanetary transfer, may require relaxation of the rendezvous constraints, especially the maximum relative velocity. Fig. 6 shows the resulting ΔV for different pericenter altitudes. On one hand, a lower pericenter altitude results in a lower Mars orbit injection ΔV. On the other hand, a higher pericenter altitude could reduce the gravity losses due to a slower orbit velocity and pericenter passage. The four 20 N thrusters accomplish the Mars orbit injection maneuver in less than three minutes, and thus only minor gravity losses are expected. Hence, a 500 km pericenter altitude is baselined.

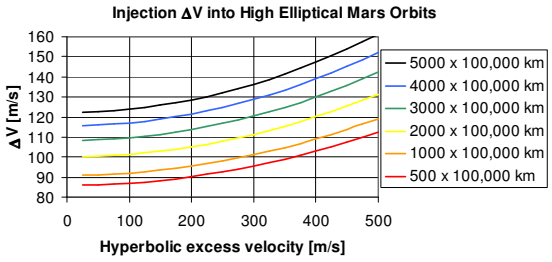

Fig. 6: Mars orbit injection ΔV

Fig. 7 shows the flight times from the SOI rim to the pericenter. Due to the low hyperbolic excess velocities, the flight times range between one and two weeks. For comparison, chemical propelled spacecraft enter the Martian SOI typically with excess velocities in the range 2-3 km/s, resulting in flight times less than three days.

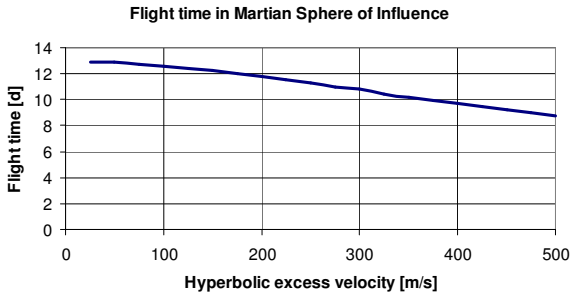

Fig. 7: Flight time from the SOI to pericenter

Spiral within Martian SOI

After injection into the high-elliptical Mars capture orbit, the spacecraft completes three revolutions (~13 d), which allows precise orbit determination to adapt the final transfer strategy to the actual orbit parameters.

We optimized minimum-duration transfers from the capture orbit to Deimos and Phobos for all spacecraft configurations. Due to the small size and the small SOIs of the Martian moons, we set rendezvous constraints of 10 km distance and 10 m/s relative velocity.

Together with the high number of required trajectory propagation steps, the demanding rendezvous constraints resulted in a very high computational effort. In a first step, we therefore conducted the trajectory optimization for an orbit rendezvous, i.e. neglecting phasing. In a second step, we optimized two trajectories for each target including the orbit phasing for verification.

The trajectory optimizer InTrance includes a detailed model of the solar system. It allows the determination of the available EP-thrust, based on the available output of the power

subsystem. The optimized transfers within the Martian SOI take into account:

- The variation of the solar flux due to the Mars moving along its elliptical orbit
- Eclipse phases due to shadowing by Mars

Typical transfers to Deimos and to Phobos are presented in Fig. 8 and Fig. 9.

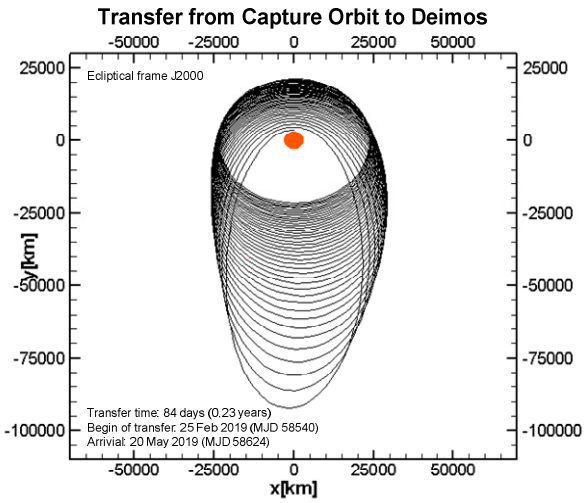

Fig. 8: Transfer of 3–RIT22LO–13.6 spacecraft from capture orbit to Deimos

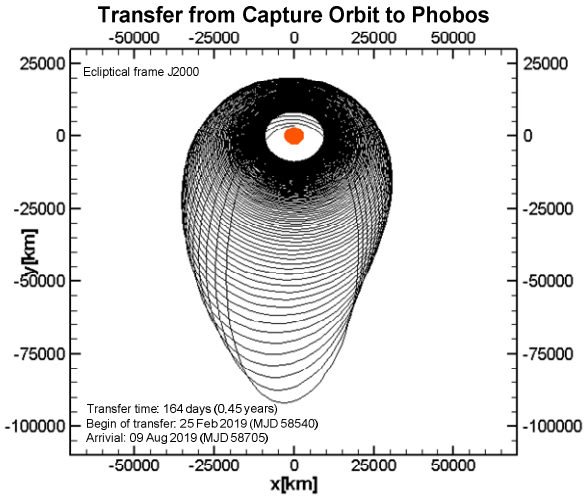

Fig. 9: Transfer of 3–RIT22LO–13.6 spacecraft from capture orbit to Phobos

Fig. 10 shows the transfer times to the various targets within the Martian SOI. First we must distinguish between transfers from the capture orbit to Deimos (blue) and to Phobos (yellow). Because Phobos is the inner moon, a spacecraft has to spiral deeper into Mars' influence domain, resulting in longer transfer times. We also optimized transfers from Deimos to Phobos (red). They used the final conditions of the capture-orbit-to-Deimos transfers as initial condition. Because Deimos and Phobos differ in their semimajor axis by only ~14,100 km, transfer duration is relatively short.

In general, Fig. 10 shows a decreasing transfer time for increasing engines count and larger power subsystem, or for both. A few exceptions have to be outlined:

- Configuration 3-PPS1350-3.8 achieves a shorter transfer time than configuration 3-PPS1350-5.2. Interestingly, this appears only for transfers from capture orbit to Deimos and Phobos. The power of both configurations is not sufficient to operate two PPS®1350-G at Mars. The longer interplanetary transfer of 3-PPS1350-3.8 (see Fig. 5), also results in a higher propellant consumption of about 85 kg. The reduced mass of 3-PPS1350-3.8 results in higher spacecraft accelerations at Mars. Thereby the spacecraft can raise the capture orbit's periapsis quicker, which increases the subsequent time span close to the periapsis. The spacecraft can thus lower the apoapsis distance during each periapsis passage more effectively.
- Although the RIT22ME spacecraft differ significantly with respect to their power system output, their transfer times from Deimos to Phobos are almost the same. This results from the minimal power requirement of the RIT22ME (4 kWe) and

the fact that even the configuration with the largest solar array is not able to support two thrusters when Mars is close to aphelion.

Tab. 3 shows how the thrust-to-power ratio decreases with increasing I_{sp}. Assuming an unchanged power subsystems, a spacecraft utilizing lower-I_{sp} engines can provide more thrust and a higher acceleration, which leads to shorter transfer times.

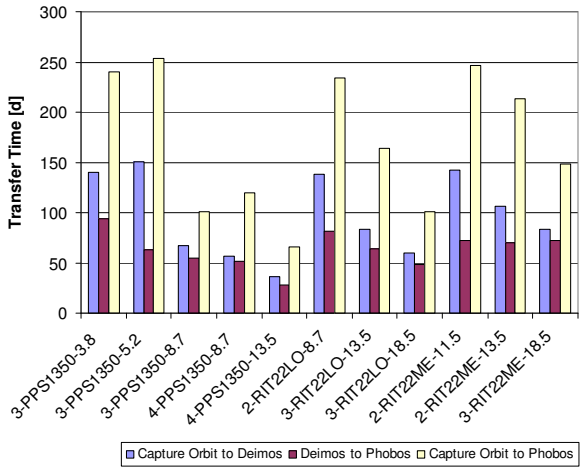

Fig. 10: Transfer times within the Martian SOI

OVERALL MISSION ASPECTS

We evaluated all investigated spacecraft configurations and the resulting optimized transfers with respect to the criteria of total mission time and possible payload mass.

Total mission time

The total mission time especially drives cost for mission operations and ground support. Furthermore, the spacecraft hardware must be qualified according to the total mission time. A short mission time is therefore beneficial to reduce the mission operation cost and the cost for hardware testing and qualification.

Fig. 11shows decreasing total mission time for larger numbers of electric engines and for larger power systems, but this effect is more pronounced for spacecraft with small EP and power subsystems.

A further aspect is the mission time difference, depending on the mission target. Dedicated Deimos missions are the shortest ones. This obviously results from the high orbit altitude of Deimos, which, compared to a dedicated Phobos mission, reduces the transfer time within the Martian SOI significantly. Combined Deimos and Phobos missions have the longest mission times, especially because two science phases are included. Each science phase consists of 30 d for orbit phasing and initial characterization of the target's gravity field. The following 120 days should be available for the scientific campaign itself.

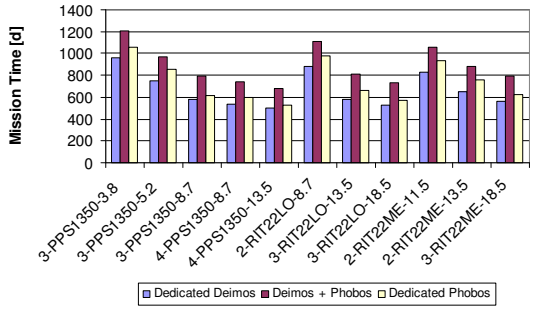

Fig. 11: Total mission time

Payload mass

Based on the launch vehicle performance and the described mission analysis, we determined payload masses for all spacecraft configurations. First, we subtracted the propellant masses, gained from the mission analysis, from the available spacecraft mass (see Tab. 4). Then, this dry mass reduces by the system margin of 20%. After that, the developed spacecraft model was used to

determine the masses of all subsystems, which were also subtracted from the dry mass (without margin). The remaining mass is available for payloads as well as its supporting structure, e.g. scan platform, and mechanisms, e.g. for lander separation. We considered the following payloads for comparison:

- Minimal instrument package: 7.5 kg [2]
- Large instrument suit: 31.5 kg [5]
- Small lander package: ~10 kg [2] (1 or more)
- Large lander: ~100 kg, e.g. Rosetta's comet lander Philae
- Rendezvous and Capture Experiement: 39.7 kg [11]

In any case, the precursor will be equipped with instruments for in situ measurements from orbit. According to used references, [2][5] in particular, the mass of such instrumentation is assumed to be in the range within 7.5 kg to 31.5 kg . If further payload mass is available, lander(s) should be included for in situ analysis of the target's surface. Another option is the inclusion of a rendezvous and capture experiment for a later Mars sample return mission. In general, the spacecraft could also carry additional propellant for hover maneuvers and/or forced orbits around the moons.

Fig. 12 shows the payload mass of the considered spacecraft configurations and targets. A significant payload mass difference is evident between the configurations with PPS®1350-G and RIT engines. The lower I_{sp} of the former (difference to RIT22LO 2,050 s) results in higher propellant masses. In principle, there is also a difference in payload mass within the two considered RIT engines, but it is smaller due to the I_{sp}-difference of only ~1,060 s.

Fig. 12 also shows a significant payload reduction for larger and heavier propulsion and power subsystems. Two exceptions are notable: The configurations 3-PPS1350-5.2 and 2-RIT22ME-13.5 have higher payload masses than the next smaller configuration. The larger solar array enables the spacecraft to avoid very long transfer durations with high ΔV-requirements (See also page 7). The achieved ΔV-reduction saves propellant mass, which allows for a higher payload mass.

In terms of payload, a dedicated Deimos mission offers the largest payload mass. The high orbit altitude of Deimos prevents the spacecraft from having to spiral very deeply into the Martian gravity field. This results in shorter transfer times and ΔVs.

The payload masses of the dedicated Phobos mission and the combined Deimos Phobos missions are almost equal. The small differences result primarily from the chemical propellant required for Deimos orbit injection in the combined mission. A combined mission to both moons has therefore the most interesting mission profile.

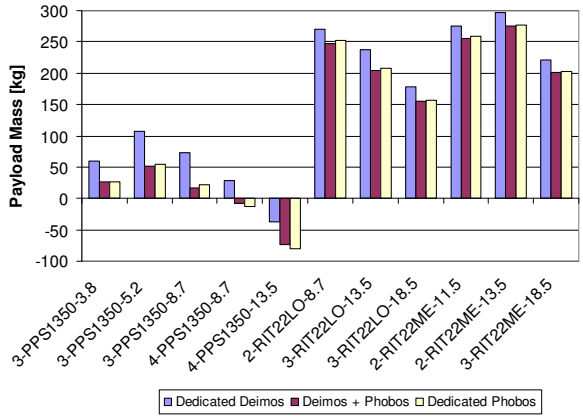

Fig. 12: Payload performance of the considered spacecraft configurations for a launch from

Baikonur and an areaspecific solar panel mass of 2.6 kg/m^2

We prefer the PPS®1350-G spacecraft configurations over the RIT-configurations due to their smaller power requirements and their resulting shorter mission times. Their payload performance is however quite low in direct comparison, but configuration 3-PPS1350-5.2 could carry a large instrument suit and probably deliver one small surface package to each Martian moon.

The RIT-22 configurations seem interesting from a payload point of view, but they require large solar arrays. Hence, such spacecraft should explore the moons' surfaces with landers instead of hovering. Those spacecrafts could even demonstrate rendezvous and capture technologies. Therefore, the rendezvous target could be ejected from a large lander on the moon's surface to demonstrate this technology for future small body missions. Considering the size of the solar array, the mission time, and the payload mass, the configuration 3-RIT22LO-13.5 is the best compromise.

In the final step of this study, we selected one spacecraft configuration for failure analysis. We expected that engine failures and solar array degradation will cause longer transfer times and also higher ΔVs, depending on the time they occur. Because the investigated PPS configurations have smaller payload masses and a lower I_{sp}, we chose the 3-RIT22LO-13.5 configuration for the following analysis.

FAILURE ANALYSIS

An EP-powered spacecraft has to operate its engines for long times. Hence, the overall probability of component failures increases with mission time. This concerns especially the electric engines and the solar array. This failure analysis investigates how underperformance of these subsystems affects the mission profile.

The mission design assumes EP for the interplanetary transfer to Mars and for the transition from the capture orbit to the target moon.
The latter phase is less critical because an EP or power subsystem's underperformance will only result in a flight time increase and probably in a slight propellant increase but the mission targets will be still accessible. In contrast, a failure during the interplanetary transfer can cause a major violation of the Mars rendezvous constraints. The spacecraft can either pass Mars at a too large distance or with too large relative velocity, or both, rendering orbit injection impossible. Consequently, our failure analysis focuses on the interplanetary transfer.

To conduct this failure analysis, we used the nominal interplanetary trajectory of the 3-RIT22LO-13.5 configuration as basis (see Fig. 13) and extracted 15 state vectors at 20 d-intervals. The vectors contained the time of flight, the actual date (MJD), the position vector, the velocity vector, and the spacecraft mass. Starting from each of these 15 new initial states, we optimized new minimum-duration transfers under the assumption of permanent engine failures or degraded solar cells. For these calculations we set the new rendezvous criteria of 5.7542×10^5 km distance and 200 m/s relative velocity at the SOI. We also increased the maximum flight time to 1,000 days.

Fig. 14 shows the change in flight time of the interplanetary transfer in dependence of the

point of time when the failure occurs. Small underperformances as the failure of one engine or a power decrease of 10% result in only small flight time increases if they occur 40 days after launch. In case of very early failures, the spacecraft tries to follow the nominal trajectory as close as possible but has problems to achieve the rendezvous constraints.

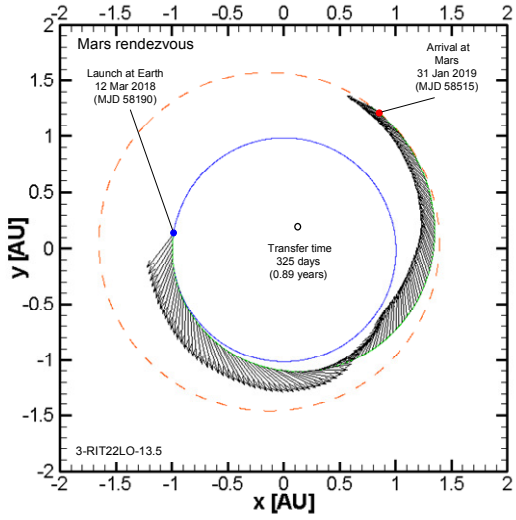

Fig. 13: Nominal interplanetary transfer trajectory of the configuration 3-RIT22LO-13.5

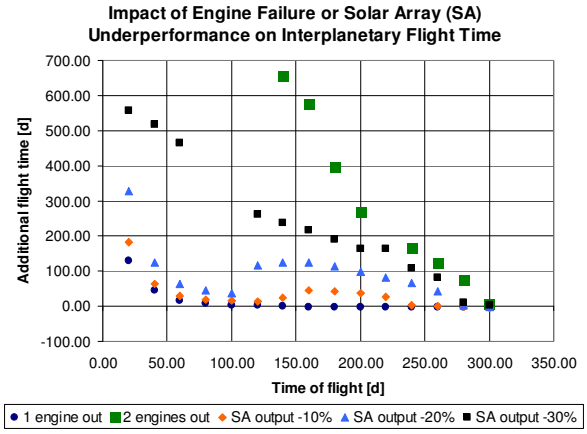

Fig. 14: Impact of engine failure or solar array degradation on the interplanetary flight time of 3-RIT22LO-13.5

The additional flight time due to power decreases of 10% and 20% shows a local minimum around 100 d of flight followed by a local maximum at ~140-160 d. This behavior results from a different control strategy. The initial states at ~100 d of flight allow an almost velocity-tangential steering of electric engines until the Mars rendezvous. In case the failure occurs later, the thrust direction has to be turned 'inwards' of the orbit to achieve the strict rendezvous constraints. Please note that a weakening of the rendezvous constraints could probably reduce the additional flight time in those cases.

More serious underperformances lead to drastically increased flight times, but those solutions still exist. Further we would like to point out that the investigated spacecraft configuration seems to have higher sensitivity to power subsystem underperformances than to engine failures. A power decrease of 30% shows higher impact on flight time than an engine failure (decrease of available thrust of 33%).

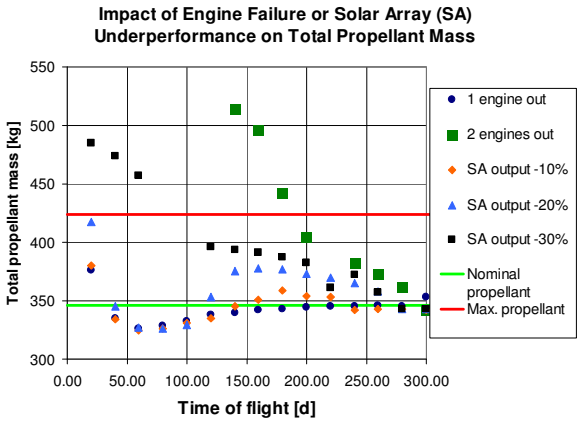

Fig. 15: Influence of engine failure or solar array degradation on the propellant mass of 3-RIT22LO-13.5

Fig. 15 shows the influence of the considered failure cases on propellant mass. For reference, the nominal and the maximal propellant masses are included. The maximal propellant mass results from the use of two 133 l tanks within the nominal mission. In principle, further propellant mass could be included in additional tanks, but this would reduce the available payload mass. However, 50 kg of additional propellant cover most of the considered failure cases. In some cases the propellant mass is even decreased due to the relaxed rendezvous constraints.

CONCLUSION AND OUTLOOK

This paper shows the feasibility of a low-thrust mission to the Martian moons. A combined Deimos-Phobos mission seems most desirable, because electric propulsion allows the visit of both targets with only a minor increase in the transfer ΔV. The mission is feasible with Snecma PPS®1350-G and the Astrium RIT-22 engines. The first option is interesting because of its significantly smaller necessary solar arrays, and the latter one offers significantly higher payload performances.

We also carried out a failure analysis for a spacecraft using RIT-22 thrusters with $I_{sp} = 3704$ s. Even if one engine stops operation (33% less thrust), or the power output of the solar array reduces by 20%, the mission can still be executed with an acceptable increase in flight time and necessary propellant mass.

REFERENCES

[1] NASA Mars Fact Sheet, http://nssdc.gsfc.nasa.gov/planetary/factsheet/marsfact.html

[2] ESA CDF Team, CDF STUDY REPORT NEO 2 A reference mission for diminishing threat from near Earth objects, CDF-39(A), ESA, 2005

[3] ESA CDF Team, CDF STUDY REPORT SANCHO Near Earth Object Monitoring Orbiter Mission, CDF-58(A), ESA, 2007

[4] ESA CDF Team, CDF Study Report Mars Electric Propulsion Study of Impact of Using Electric Propulsion on Future Mars Missions, CDF-71(A), ESA, 2008

[5] P. D'Arrigo et al., APEX Apophis Explorer, Apophis Mission Design Competition of The Planetary Society, Astrium, TP1717, 2007

[6] W. Seboldt, B. Dachwald, J. Streppel et al., Lander Mission to Europa with Solar Electric Propulsion, In: Proceedings of the 7th International Symposium on Launcher Technologies, Barcelona, Spain, 2007

[7] ESA CDF Team, CDF Study Report, LES 3 A European Robotic Lunar Mission, CDF-44(A), ESA, 2005

[8] M. Khan, Mars Precision Lander: Mission Analysis Guidelines, Issue 1 Revision 0, SRE-PAP/MREP/MPL-MAG, ESA, 2010

[9] B. Dachwald, Low-Thrust Trajectory Optimization and Interplanetary Mission Analysis Using Evolutionary Neurocontrol, Doctoral thesis, Universitaet der Bundeswehr Muenchen, Fakultaet fuer Luft- und Raumfahrt, 2004

[10] B. Dachwald, Optimization of very-low-thrust trajectories using evolutionary neurocontrol, Acta Astronautica 57, pp 175-185, 2005

[11] ESA CDF Study Team, CDF Study Report MarsGEN Orbiter and Lander Mission to Mars, CDF-88(C), ESA, 2009